Effect of chemical bonding on the magnetic stability and magnetic moment in Mn-based binary compounds

Hyun-Min Hong, Yong-Ju Kang, Joongoo Kang, E.-C. Lee, Y.-H. Kim, and K. J. Chang
Department of Physics, Korea Advanced Institute of Science and Technology, Daejeon 305-701, Korea
(Received 7 October 2004; revised manuscript received 19 July 2005; published 7 October 2005)

We study the trend of structural stability and magnetic moment for MnX (X=N, P, As, and Sb) binary compounds in the NiAs and zinc-blende structures through first-principles spin-density-functional calculations. The exchange splitting and magnetic moment are generally lower in the stable structure, which corresponds to the NiAs structure for MnP, MnAs, and MnSb whereas the zinc-blende structure for MnN. With the exception of MnN, we find the increasing trend of the stability, exchange splitting, and magnetic moment of the ferromanetic state with the anion size along the series MnP, MnAs, and MnSb. Since the N p level is much lower than other anion p levels, the Mn-N bond is more ionic, and thus MnN favors the zinc-blende structure with a lower coordination number. For MnN and MnP with small and light anions, the ground state is an antiferromagnetic state, while a ferromagnetic state is more favorable for MnAs and MnSb, which have larger equilibrium volumes and thereby reduced p-d and d-d couplings for the majority spin channel. Due to the volume and different bonding effects, MnAs and MnSb show a large exchange splitting for the d states and exhibit a nearly half-metallic behavior. The large volume increases the anion p-type character near the Fermi level, and thus the ferromagnetic state is stabilized through double exchange interactions.

DOI: 10.1103/PhysRevB.72.144408 PACS number(s): 75.50.Cc, 61.50.Ah, 71.20.Be

I. INTRODUCTION

Recently, diluted magnetic semiconductors (DMSs) have attracted much attention because of the potential use of both charge and spin of electrons for spintronic devices.[1] Several studies have demonstrated that it is indeed possible to control carrier spin dynamics and transport and design semiconductor-based magnetic devices.[2–4] Among DMSs proposed so far, III-V semiconductors doped with Mn have been mostly studied and considered as a promising material because of the compatibility with existing semiconductor processing technologies.[1,5–8] However, devices only work at temperatures far below room temperature because of the low Curie temperatrure (T_c) in these materials.[2] In as-grown $In_{1-x}Mn_xAs$ and $Ga_{1-x}Mn_xAs$ alloys, the Curie temperature is limited to about 110 K, while post-growth annealing at low temperatures can raise T_c up to 159 K.[9,10] The enhancement of T_c is attributed to the migration of Mn interstitials into the surface. In these systems, it is now believed that free holes generated by Mn ions at the cation sites are responsible for ferromagnetic interactions between Mn ions, based on the Zener mean-field model.[6] Based on the similar assumption that free holes are provided by Mn ions, a theoretical study predicted that T_c could be as high as room temperature in nitride-based DMSs such as GaMnN.[6] However, experimental results so far are quite controversial, reporting the Curie temperatures ranging from 10 to 370 K.[11–14] In contrast to theory, GaMnN samples without additional p-type dopants were shown to be n-type,[14] and no ferromagnetic state was observed in some cases.[15] Thus, it is considered that T_c might be much lower than that for the GaMnAs system, and the observed spontaneous magnetization with high T_c values is possibly due to secondary phases. Room tepmperature ferromagnetism was also reported in Mn-doped ternary compounds such as $ZnGeP_2$ and $CdGeP_2$.[16–18] However, nuclear magnetic resonance measurements indicated that the magnetic properties of $Zn_{1-x}Mn_xGeP_2$ are due to the formation of MnP clusters.[19]

In GaMnN and GaMnAs alloys, it is difficult to rule out the possibility that MnN and MnAs exist in the NiAs structure or the same crystal structure as the host material. In epitaxial growth, however, the zinc-blende structure has not been successfully formed for MnX binary compounds with X=N, P, and Sb, with a possible exception of MnAs, although zinc-blende GaMnN alloys grown on GaAs(001) have been recently reported.[20] It is known that MnAs and MnSb are stable in the hexagonal NiAs structure and both ferromagnetic at room temperature,[21] while the stable phase of MnP is the so-called MnP-type structure, which is slightly distorted from the NiAs structure.[22,23] In the ground state, MnN forms a distorted NaCl structure and exhibits an antiferromagnetic ordering up to 753 K.[24] In theoretical calculations using the full-potential linearized augmented plane wave (FLAPW) method, a tetragonally distorted antiferromagnetic NaCl structure was shown to be the stable phase of MnN.[25] Recently, Continenza and co-workers performed FLAPW calculations for various MnX binary compounds (X=P, As, Sb) in the NiAs and zinc-blende structures but not for MnN, and they showed that the magnetic properties of these compounds are strongly affected by the coordination number and chemical bonding effect.[21] Other theoretical calculations were done to search for the possible formation of the zinc-blende structure in MnAs, and showed that although zinc-blende MnAs has a ferromagnetic state, this structure cannot be stabilized either by lattice stretching or compression on GaAs surfaces, compared with the stable NiAs structure.[26] Janotti and co-workers only considered the zinc-blende structure for MnN and MnAs to gain insights into the properties of Mn impurities in GaAs and GaN, and suggested that the ferromagnetic state in GaMnAs is stabilized by free

holes through the double exchange mechanism, while Mn is inefficient to generate free holes in GaMnN.[27] Despite several theoretical attempts,[21,25–27] the chemical trend of structural stability and magnetic moment has not been systematically investigated along the series from MnN to MnSb. In addition, since it is a key issue to raise the T_c of DMSs above room temperature, it is important to understand the mechanism for ferromagnetism by deeply investigating Mn-Mn and Mn-anion interactions.

In this paper, we perform first-principles pseudopotential calculations to investigate trends in the structural and magnetic properties of the Mn*X* binary compounds (*X*=N, P, As, and Sb) in the NiAs and zinc-blende structures. Our calculations show that MnAs and MnSb have a ferromagnetic ground state in the NiAs structure, in good agreement with experiments, while MnN and MnP favor an antiferromagnetic state in the hypothetical zinc-blende and NiAs structures, respectively. Analyzing the *p-d* and *d-d* couplings for the majority spin channel, we find a trend in the magnetic stability and magnetic moment along the series; the *p-d* and *d-d* couplings decrease with the lattice constant, which enhances the stability of the ferromagnetic state and increases the magnetic moment. This trend is understood by the volume and different chemical bonding effects of the anion species. Due to the localized *d* orbitals, MnAs and MnSb show a large exchange splitting for the *d* states, and they exhibit a nearly half-metallic behavior, with larger magnetic moments. As an exceptional case, MnN is found to have a larger magnetic moment than MnP, especially in the NiAs structure, which may result from the fact that the Mn *d* states are higher in energy than the N *p* band and thus the *p-d* coupling is not so significant as in MnP. We find the chemical trend of stability that the exchange splitting and magnetic moment are generally lower in the stable structure, which corresponds to the NiAs structure for MnP, MnAs, and MnSb whereas the zinc-blende structure for MnN.

II. COMPUTATIONAL METHOD

Our calculations are based on the first-principles pseudopotential method within the local spin-density-functional approximation (LSDA)[28] and the generalized gradient approximation (GGA). We use ultrasoft pseudopotentials, including the Mn 3*p*, As 3*d*, and Sb 4*d* orbitals in the valence shell.[29] For all the atoms, we include a nonlinear partial core correction for the exchange-correlation functional to deal with the overlap between the core and valence electron densities.[30] For the GGA calculations, we use the functional form suggested by Perdew, Burke, and Ernzerhof for the exchange-correlation energy.[31] We consider the NiAs and zinc-blende structures, and investigate the stability of ferromagnetic and antiferromagnetic solutions. The antiferromagnetic state in the zinc-blende structure is modeled by forming a superlattice, where spin-up and spin-down layers are alternately stacked along the [001] direction. For the equilibrium volume of zinc-blende MnN, the antiferromagnetic spin alignment along the [001] direction is more stable by about 50 meV than for the [111] direction, while for MnP, MnAs, and MnSb, the [111] spin alignment is lower in energy by about 8, 27, and 42 meV, respectively, than for the [001] direction. The wave functions are expanded in a plane-wave basis set with a kinetic energy cutoff of 30 Ry, which ensures the total energy precision better than 1 mRy per atom for comparing ferromagnetic and antiferromagnetic states. The Brillouin-zone summation of charge densities is performed with a uniform grid of *k* points, which is generated by the Monkhorst-Pack scheme,[32] choosing 28 and 42 *k* points in the irreducible sectors for the zinc-blende and NiAs structures, respectively. For each phase, we calculate the total energies for many different volumes. For a fixed volume, we optimize all the lattice parameters including internal parameters using the conjugate gradient technique.

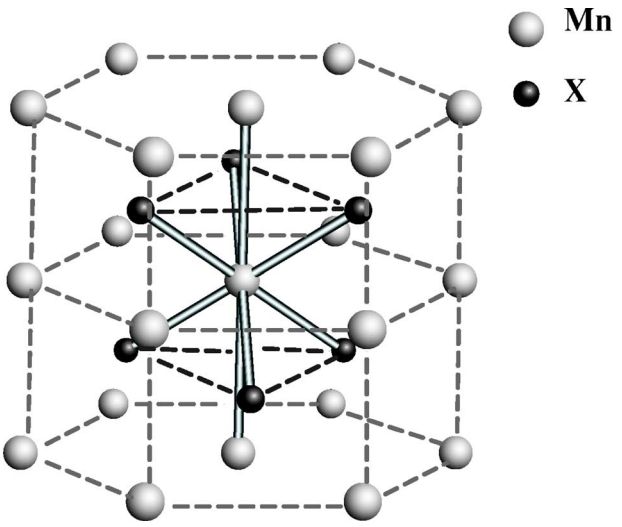

FIG. 1. (Color online) A ball-and-stick model for the NiAs structure.

III. RESULTS AND DISCUSSION

In the NiAs structure, each Mn atom forms distorted octahedral bonds with six anions and two cations, as shown in Fig. 1, while it is tetrahedrally bonded to four neighboring anions in the zinc-blende structure. The equilibrium structure of MnP is the so-called MnP type which is slightly distorted from the NiAs structure, and this compound exhibits complex magnetic behavior, antiferromagnetic at very low temperatures, ferromagnetic between 47 and 291 K, and paramagnetic at elevated temperatures.[22,23] On the other hand, MnAs and MnSb are stable in the NiAs phase and both ferromagnetic in their equilibrium structure. Although the Mn binary compounds are unstable in the zinc-blende structure, it is interesting to study the magnetic interactions of Mn ions in the tetrahedral environment because of the similar coordination in diluted $Ga_{1-x}Mn_xAs$, $Ga_{1-x}Mn_xN$, and $Zn_{1-x}Mn_xGeP_2$ alloys. Thus, we focus on the NiAs and zinc-blende structures, and compare their magnetic properties based on different bonding configurations.

Our GGA calculations for the structural parameters of the NiAs phase are listed and compared with experimental and other theoretical results in Table I. For MnP, MnAs, and MnSb, we find that the lattice constants (a) and axial ratios

TABLE I. Calculated lattice constants (a), axial ratios (c/a), Mn-anion ($d_{\text{Mn-anion}}$) and Mn-Mn distances ($d_{\text{Mn-Mn}}$), equilibrium volumes (V_o), bulk moduli (B_o), and magnetic moments (μ) are listed for the ferromagnetic state of MnN, MnP, MnAs, and MnSb in the NiAs structure.

	a (Å)	c/a	$d_{\text{Mn-anion}}$ (Å)	$d_{\text{Mn-Mn}}$ (Å)	V_o (Å^3)	B_o (GPa)	μ (μ_B)	
MnN	2.808	1.77	2.044	2.487	16.98	175	2.26	Our work
MnP	3.381	1.57	2.360	2.653	26.27	93	2.04	Our work
	3.386	1.62		2.68			2.04	Other work[a]
MnAs	3.693	1.49	2.535	2.751	32.49	70	3.06	Our work
	3.704	1.49		2.84			3.15	Other work[a]
	3.7	1.54					3.4	Experiment[b]
MnSb	4.082	1.38	2.744	2.815	40.65	66	3.23	Our work
	4.128	1.35		2.89			3.25	Other work[a]
	4.12[c]	1.40[c]					3.55–3.50[a]	Experiment

[a]Reference 21.
[b]Reference 26.
[c]Reference 33.

(c/a) are very similar to previous FLAPW-GGA calculations.[21] For MnAs and MnSb, where experimental data are available, we also find good agreements for a with errors less than 1%. Along the series from MnN to MnSb in the NiAs structure, the Mn-anion distances are 2.044, 2.360, 2.535, and 2.744 Å, respectively, following the trend of the anion ionic radii. The Mn-Mn nearest neighbor distances similarly increase with the anion size, i.e., $d_{\text{M-Mn}}$=2.487, 2.653, 2.751, and 2.815 Å along the series. However, the increasing rates are lower because the c/a ratios decrease simultaneouly, resulting in the effective coordination number of 8 for MnAs and MnSb. For MnP in the NiAs structure, the calculated Mn-Mn distance of 2.653 Å is close to the measured value of 2.696 Å in the stable MnP-type structure.[34] We find that MnSb has similar Mn-anion and Mn-Mn bond distances, while the Mn-Mn bond distance is larger by about 20% than for the Mn-anion bond in MnN.

In the zinc-blende structure, the equilibrium lattice constants agree well with other calculations, with errors less than 1%, as listed in Table II. We find that the lattice constants are not very far from those of related Ga compounds; the atomic volume of wurtzite GaN is used to estimate the lattice constant for the zinc-blende structure. Along the series from MnN to MnSb, the Mn-anion bond distances are 1.860, 2.292, 2.467, and 2.671Å, which are reduced by 3%–9 %, compared with those in the NiAs structure. For MnAs, the equilibrium lattice constant for the zinc-blende structure is estimated to be 5.697 Å, smaller by about 3% than that (5.89 Å) predicted from the linear extrapolation of the experimental lattice constants of $Ga_{1-x}Mn_xAs$ alloys.[35] However, our estimate is in good agreement with other pseudopotential[26] and FLAPW[21,27] calculations, as shown in Table II. At this point, it is not clear whether the underestimation of the lattice parameter is due to the use of the local-density-functional approximation or the incorrect linear extrapolation of the measured GaMnAs lattice contants for $x \rightarrow 1$. On the other hand, the Mn-Mn bond distances are 3.037, 3.742, 4.028, and 4.361 Å, respectively, and these values are greatly

TABLE II. Calculated lattice constants (a), Mn-anion ($d_{\text{Mn-anion}}$), and Mn-Mn distances ($d_{\text{Mn-Mn}}$), equilibrium volumes (V_o), bulk moduli (B_o), and magnetic moments (μ) are listed for the ferromagnetic state of MnN, MnP, MnAs, and MnSb in the zinc-blende structure. The measured lattice constants of related zinc-blende Ga compounds are also given, while a hypothetical zinc-blende structure is assumed for GaN, with the same atomic volume as that of wurtzite GaN.

	a (Å)	$d_{\text{Mn-anion}}$ (Å)	$d_{\text{Mn-Mn}}$ (Å)	a_{GaX} (Å)	V_o (Å^3)	B_o (GPa)	μ (μ_B)	
MnN	4.295	1.860	3.037	4.489	19.81	239	1.18	Our work
	4.339						1.2	Other work[a]
MnP	5.292	2.292	3.742	5.451	37.04	42	2.91	Our work
	5.308		3.75				2.73	Other work[b]
MnAs	5.697	2.467	4.028	5.654	46.23	41	3.87	Our work
	5.695						3.63	Other work[a]
	5.643		3.99				3.75	Other work[b]
MnSb	6.168	2.671	4.361	6.118	58.65	48	4.0	Our work
	6.166		4.36				3.77	Other work[b]

[a]Reference 27.
[b]Reference 21.

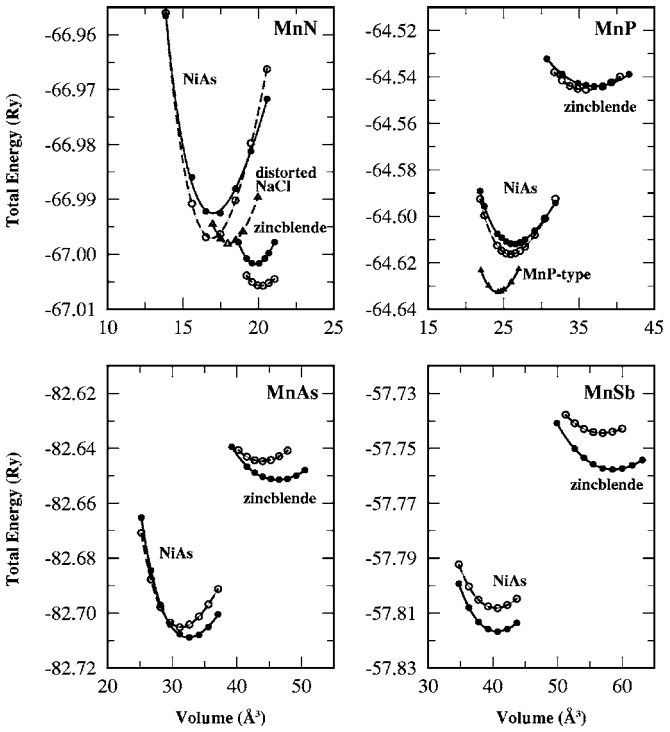

FIG. 2. The total energies vs volume for MnN, MnP, MnAs, and MnSb in the NiAs and zinc-blende structures. Filled and empty circles denote the ferromagnetic and antiferromagnetic states, respectively. In MnN, empty triangles represent the antiferromagnetic state for the distorted NaCl structure, and filled triangles in MnP denote the ferromagnetic state for the orthorhombic MnP-type structure.

increased due to the reduced coordination number and increased crystal volume. As going from MnN to MnSb, the increase of the Mn-Mn bond distance is more significant, indicating that Mn *d*-*d* interactions are significantly weakened.

The total energies for the NiAs and zinc-blende structures are plotted as a function of volume in Fig. 2. For both the structures, we examine the stability of ferromagnetic (FM) and antiferromagnetic (AFM) solutions. For a fixed volume, we optimize the structural parameters including a and c/a. From the Murnaghan equation of state,[36] the equilibrium volume (V_o) and bulk modulus (B_o) are calculated and listed in Tables I and II. For all the compounds, the zinc-blende structure has a larger equilibrium volume than the NiAs structure. However, our calculations show that the NiAs structure is generally lower in energy by 0.06–0.07 Ry per formula unit than for the zinc-blende structure, with the exception of MnN, in which the zinc-blende structure is more stable by about 0.01 Ry per formula unit. The stability of the zinc-blende structure in MnN is attributed to the fact that the N *p* level is much lower than other anion *p* levels, and thus the Mn-N bond is more ionic but of mixed type,[25] which favors the zinc-blende structure with a lower coordination number. In addition, since the Mn-Mn distance is much smaller in the NiAs structure, the Coulomb repulsive energy is more enhanced by the overlap of the Mn *d* orbitals, as compared to the zinc-blende structure. For the tetragonally distorted NaCl structure in MnN, we find that the AFM phase with spin-up and spin-down layers alternated along the c axis is more stable than for the FM state, and estimate the equilibrium lattice constants of $a=4.18$ Å and $c=4.04$ Å, in good agreement with experiments.[24] However, the distorted NaCl structure is higher in energy than the zinc-blende structure, as shown in Fig. 2. At this point, it is not clear whether the discrepancy between the theoretical and experimental results for the globally stable structure is caused by using the LSDA or neglecting the possible effect of defects on stability. In MnP, the ground state below the Néel temperature of 47 K is a screw antiferromagnetic state in the orthorhombic MnP-type structure.[22,23] Since it is difficult to calculate the energy for the screw antiferromagnetic state, we consider the ferromagnetic spin configuration. In this case, the MnP-type structure is found to be more stable than for both the NiAs and zinc-blende structure, as shown in Fig. 2, and its equilibrium volume is calculated to be 24.23 Å^3, close to the measured value of 24.68 Å^3.[34] For MnAs and MnSb, the FM state is more favorable in the NiAs structure, in good agreement with experiments, while the AFM state is energetically more stable for MnN and MnP. These results indicate that the stability of the FM state is enhanced for large Mn-Mn distances.

We discuss the electronic properties of the Mn-based compounds in both the NiAs and zinc-blende structures. The calculated densities of states (DOS) projected onto the Mn and anion sites are drawn and compared for the equilibrium volumes of the ferromagnetic state in Fig. 3. From the band structure, we find that the electronic and magnetic properties are closely related to the anion size and different bonding effect. In the NiAs structure, we find that for MnN, the Mn *d* band is well separated from the anion *p* band, since the anion *p* level is lower than the Mn *d* level. In this material, the *d*-*d* coupling is stronger due to the small Mn-Mn distance, thus, a small exchange splitting occurs between the majority and minority channels of the Mn *d* states. On the other hand, MnP, MnAs, and MnSb show similar projected densities of states, exhibiting stronger *p*-*d* hybridizations than for MnN. As going from MnP to MnSb, since the Mn-anion distance as well as the anion *p* levels relative to the Mn *d* levels increase, the *p*-*d* hybridization is relatively weakened. This feature is clearly seen by the trend of the valence band with the anion size. In MnP, the main peaks of the Mn *d* band are separated by about 2.2 eV for the majority spin channel, while this energy separation decreases to 1.3 eV for MnAs and then 0.7 eV for MnSb. The main *d*-band width for the majority spin channel also decreases from 5.4 to 4.2 eV along the series. Analyzing the states crossing the Fermi level, we note that the anion *p* character appears more strongly as the anion size increases, while the Mn *d* character is dominant near the Fermi level for MnN. For MnAs and MnSb, the *d*-*d* hybridization is lowered by the increase of the Mn-Mn distances due to the larger volume size. This effect enhances the exchange splitting between the majority and minority channels, leading to a nearly half-metallic behavior and thereby larger magnetic moments.

In the zinc-blende structure, the calculated densities of states are similar to those for the NiAs structure. However, since the Mn-Mn distances are much larger due to the in-

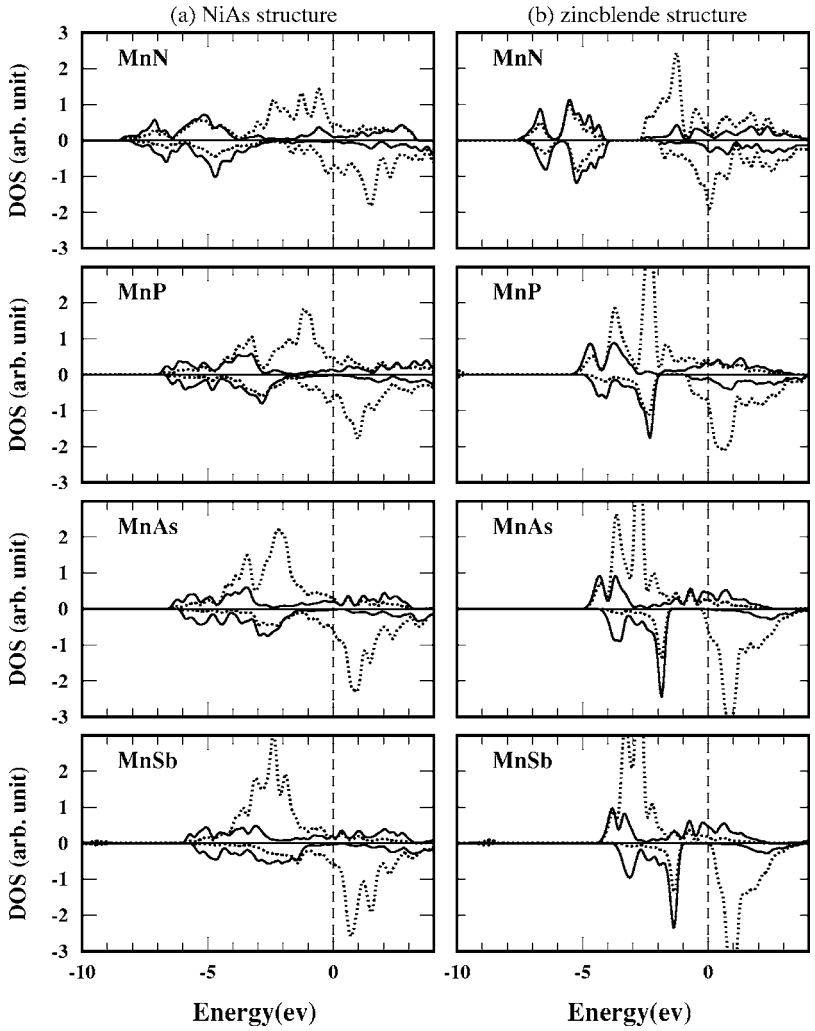

FIG. 3. The densities of states (DOS) projected onto the atomic sites at the equilibrium volumes of MnN, MnP, MnAs, and MnSb in the (a) NiAs and (b) zinc-blende structures. Solid and dotted lines denote the anion *p*- and Mn *d*-projected DOSs, respectively.

creased equilibrium volumes and reduced coordination number, the Mn *d* orbitals are more strongly localized, weakening the *d*-*d* hybridization. In fact, we find that the Mn *d* states are lowered, with narrower bandwidths, and thus the half-metallic behavior is more pronounced, consistent with previous calculations.[21,26] Due to the increased exchange interaction, the magnetic moments are found to be greatly enhanced, as compared to the NiAs structure.

In previous calculations, double exchange and superexchange interactions were used to analyze the magnetic stability of Mn binary compounds, especially MnN and MnAs.[27] For the zinc-blende structure, MnN was shown to favor the AFM state, while the FM state is stabilized for MnAs, consistent with our calculations. In MnN, because the anion *p* band is fully occupied, which suppresses the number of *p*-like holes, the double exchange interaction is weakened, compared with the antiferromagnetic superexchange interaction. We also confirm that the states near the Fermi level have more Mn *d* character for MnN and MnP. In MnP, the two total energy curves for the FM and AFM states are crossed as the volume increases, stabilizing the FM state (see Fig. 2). When the volume of MnP increases to the equilibrium volume for MnAs, the Mn *d*-projected density of states resembles that for MnAs, as shown in Fig. 4. These results indicate that the magnetic transition from the AFM to FM state in MnP at 47 K may be related to the volume expansion by temperature. For MnAs and MnSb, the anion *p* character is enhanced near the Fermi level, whereas the *d* band for the majority spin channel is lowered. The increase of *p*-like carriers increases the double exchange interaction, and stabilizes the FM state against the AFM superexchange interaction. In fact, the energy difference between the AFM and FM states increases with the anion size, as shown in Fig. 5(a). In addi-

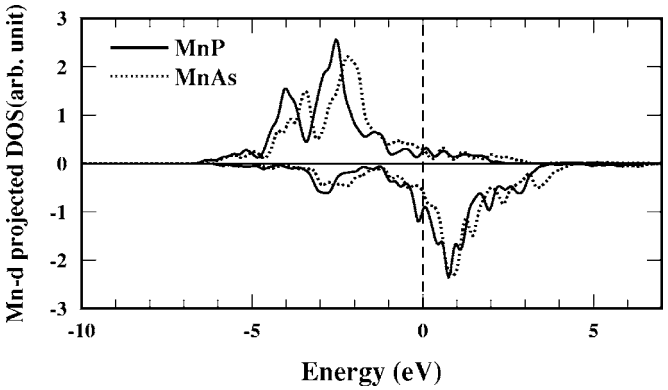

FIG. 4. The Mn *d*-projected density of states of NiAs-MnP at a volume of 31.86 Å^3 is compared with that for MnAs at the equilibrium volume.

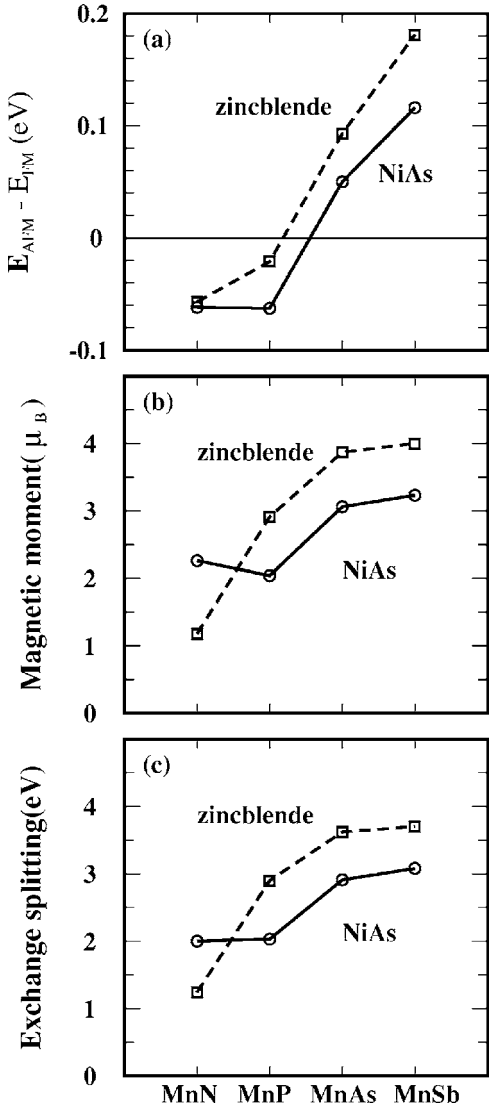

FIG. 5. (a) The energy differences between the antiferromagnetic and ferromagnetic states, (b) the magnetic moments, and (c) the exchange splittings of the Mn *d* states at the equilibrium volumes of MnN, MnP, MnAs, and MnSb in the NiAs and zinc-blende structures.

tion, for the zinc-blende structure, we find that the difference between the FM and AFM equilibrium lattice constants decreases as going from MnSb to MnP, and then its sign is reversed for MnN. This trend indicates that the ground state has a larger lattice constant and thus favors a higher spin state, with the exception of MnP. In MnN, the AFM state with the larger lattice constant is stabilized due to the stronger superexchange interaction. As going from MnN to MnSb, the Mn *d* level is relatively lowered and the anion *p* band tends to be partially occupied. Then, the enhanced double exchange mechanism leads to the ferromagnetic state which has the larger lattice constant. The screening effect by the anion *p* orbitals is smaller for MnN and MnP, which have more Mn *d* character near the Fermi level. Thus, it is expected that the magnetic properties of these compounds will be more strongly affected by including a proper correlation

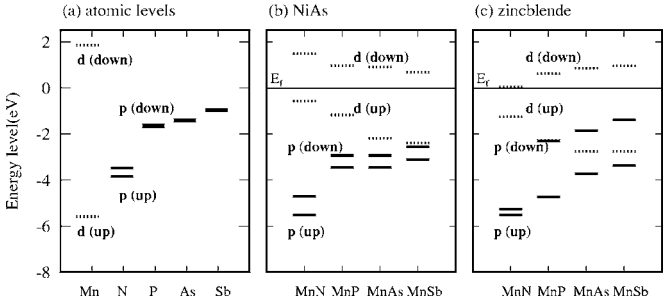

FIG. 6. (a) The atomic energy levels of the Mn, N, P, As, and Sb atoms are compared with each other. In the compounds, the Mn *d* (dotted) and anion *p* (solid) levels in the (b) NiAs and (c) zinc-blende structures are drawn with the Fermi level (E_f) set to zero. For each level, two lines denote the main peaks for the majority and minority bands.

energy such as an LSDA+U treatment, as compared to MnAs and MnSb.

The magnetic moments are calculated by projecting the wave functions onto the atomic orbitals at each site and drawn for the NiAs and zinc-blende structures in Fig. 5(b). We find an increasing trend with the anion size except for MnN in the NiAs structure. Previous calculations suggested that this trend have its origin in *d-d* and *p-d* hybridizations.[21] Since the equilibrium volume increases along the series, the increased Mn-Mn distance weakens the *d-d* overlap and makes the Mn *d* orbitals more localized. The *d* orbital localization enhances the exchange splitting of the Mn *d* states, as shown in Fig. 5(c), and it eventually leads to higher magnetic moments. For zinc-blende MnAs and MnSb, the magnetic moments are calculated to be 3.87 and 4.0 μ_B, respectively, thus, Mn-Mn interactions are considered to be nearly in the atomic limit.

In the NiAs structure, the magnetic moment of MnN is slightly larger than that for MnP, as shown in Fig. 5(b). To see the origin for this exceptional case for the chemical trend, we analyze the *p-d* hybridization. As the anion size decreases, the Mn-anion distance also decreases. Then, the *p-d* hybridization is enhanced, and the magnetic moment is generally reduced. In MnN, however, the anion *p* level is much lower than that for MnP, as shown in Fig. 6. Thus, the *p-d* hybridization is not so significant as expected, especially for the NiAs structure, and the magnetic moment of MnN is not significantly reduced, compared with the zinc-blende structure. For the distorted NaCl structure of MnN, the local magnetic moment on the Mn ion in the AFM phase is calculated to be about 3.2 μ_B, in good agreement with the measured value of 3.3 μ_B.[24]

IV. CONCLUSION

In conclusion, we have studied the structural and magnetic properties of the Mn-based binary compounds in the NiAs and zinc-blende structures through first-principles spin-density functional calculations. The exchange splitting and magnetic moment are generally lower in the stable structure, which corresponds to the NiAs structure for MnP, MnAs, and MnSb whereas the zinc-blende structure for MnN. With the

exception of MnN, we find the increasing trend of the magnetic stability, exchange splitting, and magnetic moment along the series MnP, MnAs, and MnSb. This feature is attributed to the different bonding properties of the anion species with the Mn ions, which affect the *p*-*d* and *d*-*d* hybridizations. As the anion becomes larger, the large volume lowers the *d*-*d* hybridization and increases the exchange interaction for the Mn *d* states, resulting in a nearly half-metallic behavior. Our results show that MnN and MnP are both antiferromagnetic in their equilibrium structure, while the ferromagnetic spin alignment is more favorable, as going to MnAs and MnSb, in good agreement with experiments. From the analysis of the states near the Fermi level, the *p* character is enhanced for the heavier anions, and this increase of *p*-type carriers leads to the increase of the double-exchange interaction, which stabilizes the ferromagnetic state.

ACKNOWLEDGMENT

This work was supported through the National Science and Technology Program (Grant No. M1-0213-04-0001).

[1] H. Ohno, Science **281**, 951 (1998).
[2] Y. Ohno, D. K. Young, B. Beschoten, F. Matsukura, H. Ohno, and D. D. Awschalom, Nature (London) **402**, 790 (1999).
[3] H. Ohno, D. Chiba, F. Matsukura, T. Omiya, E. Abe, T. Dietl, Y. Ohno, and K. Ohtani, Nature (London) **408**, 944 (2000).
[4] G. Prinz, Science **282**, 1660 (1998).
[5] H. Ohno, J. Cryst. Growth **251**, 285 (2003).
[6] T. Dietl, H. Ohno, F. Matsukura, J. Cibert, and D. Ferrand, Science **287**, 1019 (2000).
[7] K. M Yu, W. Walukiewicz, T. Wojtowicz, I. Kuryliszyn, X. Liu, Y. Sasaki, and J. K. Furdyna, Phys. Rev. B **65**, 201303(R) (2002).
[8] A. Koeder, W. Limmer, S. Frank, W. Schoch, V. Avrutin, R. Sauer, A. Waag, K. Zuern, and P. Ziemann, Appl. Phys. Lett. **85**, 783 (2004).
[9] K. C. Ku, S. J. Potashnik, R. F. Wang, M. J. Seong, E. Johnston-Halperin, R. C. Meyers, S. H. Chun, A. Mascarenhas, A. C. Gossard, D. D. Awschalom, P. Schiffer, and N. Samarth, Appl. Phys. Lett. **82**, 2302 (2003).
[10] K. W. Edmonds, P. Boguslawski, K. Y. Wang, R. P. Campion, S. N. Novikov, N. R. S. Farley, B. L. Gallagher, C. T. Foxon, M. Sawicki, T. Dietl, M. B. Nardelli, and J. Bernholc, Phys. Rev. Lett. **92**, 037201 (2004).
[11] M. E. Overberg, C. R. Abernathy, S. J. Pearton, N. A. Theodoropoulou, K. T. McCarthy, and A. F. Hebard, Appl. Phys. Lett. **79**, 1312 (2001).
[12] M. L. Reed, N. A. El-Masry, H. H. Stadelmaier, M. K. Ritums, M. J. Reed, C. A. Parker, J. C. Roberts, and S. M. Bedair, Appl. Phys. Lett. **79**, 3473 (2001).
[13] N. Theodoropoulou, A. F. Hebard, M. E. Overberg, C. R. Abernathy, S. J. Pearton, S. N. G. Chu, and R. G. Wilson, Appl. Phys. Lett. **78**, 3475 (2001).
[14] G. T. Thaler, M. E. Overberg, B. Gila, R. Frazier, C. R. Abernathy, S. J. Pearton, J. S. Lee, S. Y. Lee, Y. D. Park, Z. G. Khim, J. Kim, and F. Ren, Appl. Phys. Lett. **80**, 3964 (2002).
[15] D. Dhar, O. Brandt, A. Trampert, L. Däweritz, K. J. Friedland, K. H. Ploog, J. Keller, B. Beschoten, and G. Güntherodt, Appl. Phys. Lett. **82**, 2077 (2003).
[16] K. Sato, G. A. Medvedkin, T. Nishi, Y. Hasegawa, R. Misawa, K. Hirose, and T. Ishibashi, J. Appl. Phys. **89**, 7027 (2001).
[17] G. A. Medvedkin, T. Ishibashi, T. Nishi, K. Hayata, Y. Hasegawa, and K. Sato Jpn. J. Appl. Phys., Part 2 **39**, L949 (2000).
[18] S. Cho, S. Choi, G. B. Cha, S. C. Hong, Y. Kim, Y. J. Zhao, A. J. Freeman, J. B. Ketterson, B. J. Kim, Y. C. Kim, and B. C. Choi, Phys. Rev. Lett. **88**, 257203 (2002).
[19] T. Hwang, J. H. Shim, and S. Lee, Appl. Phys. Lett. **83**, 1809 (2003).
[20] S. V. Novikov, K. W. Edmonds, A. D. Giddings, K. Y. Wang, C. R. Staddon, R. P. Campion, B. L. Gallagher, and C. T. Foxon, Semicond. Sci. Technol. **19**, L13 (2004).
[21] A. Continenza, S. Picozzi, W. T. Geng, and A. J. Freeman, Phys. Rev. B **64**, 085204 (2001).
[22] H. Okuda, S. Senba, H. Sato, K. Shimada, H. Namatame, and M. Taniguchi, J. Electron Spectrosc. Relat. Phenom. **101-103**, 657 (1999).
[23] T. Komatsubara, T. Suzuki, and E. Hirahara, J. Phys. Soc. Jpn. **28**, 317 (1970).
[24] K. Suzuki, T. Kaneko, H. Yosida, Y. Obi, H. Fujimori, and H. Morita, J. Alloys Compd. **306**, 66 (2000); K. Suzuki, Y. Yamaguchi, T. Kaneko, H. Yoshida, Y. Obi, H. Fujimori, and H. Morita, J. Phys. Soc. Jpn. **70**, 1084 (2001).
[25] B. R. Sahu and L. Kleinman, Phys. Rev. B **68**, 113101 (2003).
[26] S. Sanvito and N. A. Hill, Phys. Rev. B **62**, 15553 (2000).
[27] A. Janotti, S.-H. Wei, and L. Bellaiche, Appl. Phys. Lett. **82**, 766 (2003).
[28] P. Hohenberg and W. Kohn, Phys. Rev. **136**, B864 (1964); W. Kohn and L. J. Sham, *ibid.* **140**, A1133 (1965).
[29] D. Vanderbilt, Phys. Rev. B **41**, R7892 (1990).
[30] S. G. Louie, S. Froyen, and M. L. Cohen, Phys. Rev. B **26**, 1738 (1982).
[31] J. P. Perdew, K. Burke, and M. Ernzerhof, Phys. Rev. Lett. **77**, 3865 (1996).
[32] H. J. Monkhorst and J. D. Pack, Phys. Rev. B **13**, 5188 (1976).
[33] R. W. G. Wyckoff, *Crystal Structures*, 2nd ed. (Interscience, New York, 1960), Vol. 1.
[34] A. Yanase and A. Hasegawa, J. Phys. C **13**, 1989 (1980).
[35] H. Ohno, J. Magn. Magn. Mater. **200**, 110 (1999).
[36] F. D. Murnaghan, Proc. Natl. Acad. Sci. U.S.A. **30**, 244 (1944).